Research Article | Vol. 8, No. 8 | 1 Aug 2017 | BIOMEDICAL OPTICS EXPRESS 3735
Biomedical Optics EXPRESS

Visualization of laser tattoo removal treatment effects in a mouse model by two-photon microscopy

Won Hyuk Jang,[1,4] Yeoreum Yoon,[2,4] Wonjoong Kim,[3] Soonjae Kwon,[2] Seunghun Lee,[3] Duke Song,[3] Jong Woon Choi,[3] and Ki Hean Kim[1,2,*]

[1]*Division of Integrative Biosciences and Biotechnology, Pohang University of Science and Technology, San 31, Hyoja-dong, Nam-gu, Pohang, Gyeongbuk 790-784, South Korea*
[2]*Department of Mechanical Engineering, Pohang University of Science and Technology, San 31, Hyoja-dong, Nam-gu, Pohang, Gyeongbuk 790-784, South Korea*
[3]*Lutronic Center, 219 Sowon-ro, Deogyang-gu, Goyang-si, Gyeonggi-do, 412-223, South Korea*
[4]*Authors contributed equally*
[*]*kiheankim@postech.ac.kr*

Abstract: Laser tattoo removal is an effective method of eliminating tattoo particles in the skin. However, laser treatment cannot always remove the unwanted tattoo completely, and there are risks of either temporary or permanent side effects. Studies using preclinical animal models could provide detailed information on the effects of laser treatment in the skin, and might help to minimize side effects in clinical practices. In this study, two-photon microscopy (TPM) was used to visualize the laser treatment effects on tattoo particles in both phantom specimens and *in vivo* mouse models. Fluorescent tattoo ink was used for particle visualization by TPM, and nanosecond (ns) and picosecond (ps) lasers at 532 nm were used for treatment. In phantom specimens, TPM characterized the fragmentation of individual tattoo particles by tracking them before and after the laser treatment. These changes were confirmed by field emission scanning electron microscopy (FE-SEM). TPM was used to measure the treatment efficiency of the two lasers at different laser fluences. In the mouse model, TPM visualized clusters of tattoo particles in the skin and detected their fragmentation after the laser treatment. Longitudinal TPM imaging observed the migration of cells containing tattoo particles after the laser treatment. These results show that TPM may be useful for the assessment of laser tattoo removal treatment in preclinical studies.

OCIS codes: (180.4315) Nonlinear microscopy; (170.3880) Medical and biological imaging; (110.0180) Microscopy; (170.1870) Dermatology;

References and links

1. S. Choudhary, M. L. Elsaie, A. Leiva, and K. Nouri, "Lasers for tattoo removal: a review," Lasers Med. Sci. **25**(5), 619–627 (2010).
2. S. D. Shah and S. J. Aurangabadkar, "Newer trends in laser tattoo removal," J. Cutan. Aesthet. Surg. **8**(1), 25–29 (2015).
3. K. Sardana, R. Ranjan, and S. Ghunawat, "Optimising laser tattoo removal," J. Cutan. Aesthet. Surg. **8**(1), 16–24 (2015).
4. O. Reiter, L. Atzmony, L. Akerman, A. Levi, R. Kershenovich, M. Lapidoth, and D. Mimouni, "Picosecond lasers for tattoo removal: a systematic review," Lasers Med. Sci. **31**(7), 1397–1405 (2016).
5. S. J. Aurangabadkar, "Shifting paradigm in laser tattoo removal," J. Cutan. Aesthet. Surg. **8**(1), 3–4 (2015).
6. L. Izikson, W. Farinelli, F. Sakamoto, Z. Tannous, and R. R. Anderson, "Safety and effectiveness of black tattoo clearance in a pig model after a single treatment with a novel 758 nm 500 picosecond laser: a pilot study," Lasers Surg. Med. **42**(7), 640–646 (2010).
7. N. Saedi, A. Metelitsa, K. Petrell, K. A. Arndt, and J. S. Dover, "Treatment of tattoos with a picosecond alexandrite laser: a prospective trial," Arch. Dermatol. **148**(12), 1360–1363 (2012).
8. V. Ross, G. Naseef, G. Lin, M. Kelly, N. Michaud, T. J. Flotte, J. Raythen, and R. R. Anderson, "Comparison of responses of tattoos to picosecond and nanosecond Q-switched neodymium: YAG lasers," Arch. Dermatol. **134**(2), 167–171 (1998).

#292763 https://doi.org/10.1364/BOE.8.003735
Journal © 2017 Received 14 Apr 2017; revised 19 Jun 2017; accepted 16 Jul 2017; published 20 Jul 2017

Biomedical Optics EXPRESS

9. Y. Eklund and A. Troilius Rubin, "Laser Tattoo Removal, Precautions, and Unwanted Effects," in *Tattooed Skin and Health*, J. Serup, N. Kluger, W. Bäumler, ed. (Karger Publishers, 2015)
10. W. Kirby, A. Desai, T. Desai, F. Kartono, and P. Geeta, "The Kirby-Desai Scale: A Proposed Scale to Assess Tattoo-removal Treatments," J. Clin. Aesthet. Dermatol. **2**(3), 32–37 (2009).
11. N. Khunger, A. Molpariya, and A. Khunger, "Complications of tattoos and tattoo removal: Stop and think before you ink," J. Cutan. Aesthet. Surg. **8**(1), 30–36 (2015).
12. J. M. Handley, "Adverse events associated with nonablative cutaneous visible and infrared laser treatment," J. Am. Acad. Dermatol. **55**(3), 482–489 (2006).
13. A. Klein, I. Rittmann, K.-A. Hiller, M. Landthaler, and W. Bäumler, "An Internet-based survey on characteristics of laser tattoo removal and associated side effects," Lasers Med. Sci. **29**(2), 729–738 (2014).
14. D. Huang, E. A. Swanson, C. P. Lin, J. S. Schuman, W. G. Stinson, W. Chang, M. R. Hee, T. Flotte, K. Gregory, C. A. Puliafito, and et, "Optical coherence tomography," Science **254**(5035), 1178–1181 (1991).
15. H. Morsy, M. Mogensen, L. Thrane, and G. B. Jemec, "Imaging of intradermal tattoos by optical coherence tomography," Skin Res. Technol. **13**(4), 444–448 (2007).
16. D. J. Cuccia, F. Bevilacqua, A. J. Durkin, and B. J. Tromberg, "Modulated imaging: quantitative analysis and tomography of turbid media in the spatial-frequency domain," Opt. Lett. **30**(11), 1354–1356 (2005).
17. F. R. Ayers, D. J. Cuccia, K. M. Kelly, and A. J. Durkin, "Wide-field spatial mapping of in vivo tattoo skin optical properties using modulated imaging," Lasers Surg. Med. **41**(6), 442–453 (2009).
18. M. Rajadhyaksha, S. González, J. M. Zavislan, R. R. Anderson, and R. H. Webb, "In vivo confocal scanning laser microscopy of human skin II: advances in instrumentation and comparison with histology," J. Invest. Dermatol. **113**(3), 293–303 (1999).
19. K. O'goshi, C. Suihko, and J. Serup, "In vivo imaging of intradermal tattoos by confocal scanning laser microscopy," Skin Res. Technol. **12**(2), 94–98 (2006).
20. D. Débarre, W. Supatto, A.-M. Pena, A. Fabre, T. Tordjmann, L. Combettes, M.-C. Schanne-Klein, and E. Beaurepaire, "Imaging lipid bodies in cells and tissues using third-harmonic generation microscopy," Nat. Methods **3**(1), 47–53 (2006).
21. J. Squier, M. Müller, G. Brakenhoff, and K. R. Wilson, "Third harmonic generation microscopy," Opt. Express **3**(9), 315–324 (1998).
22. M. R. Tsai, C. Y. Lin, Y. H. Liao, and C. K. Sun, "Applying tattoo dye as a third-harmonic generation contrast agent for in vivo optical virtual biopsy of human skin," J. Biomed. Opt. **18**(2), 026012 (2013).
23. W. Denk, J. H. Strickler, and W. W. Webb, "Two-photon laser scanning fluorescence microscopy," Science **248**(4951), 73–76 (1990).
24. W. R. Zipfel, R. M. Williams, and W. W. Webb, "Nonlinear magic: multiphoton microscopy in the biosciences," Nat. Biotechnol. **21**(11), 1369–1377 (2003).
25. B. R. Masters, P. T. So, and E. Gratton, "Multiphoton excitation fluorescence microscopy and spectroscopy of in vivo human skin," Biophys. J. **72**(6), 2405–2412 (1997).
26. M. Balu, C. B. Zachary, R. M. Harris, T. B. Krasieva, K. König, B. J. Tromberg, and K. M. Kelly, "In vivo multiphoton microscopy of basal cell carcinoma," JAMA Dermatol. **151**(10), 1068–1074 (2015).
27. T. R. Mempel, S. E. Henrickson, and U. H. Von Andrian, "T-cell priming by dendritic cells in lymph nodes occurs in three distinct phases," Nature **427**(6970), 154–159 (2004).
28. B. G. Yipp and P. Kubes, "Antibodies against neutrophil LY6G do not inhibit leukocyte recruitment in mice in vivo," Blood **121**(1), 241–242 (2013).
29. T. Wang, W. H. Jang, S. Lee, C. J. Yoon, J. H. Lee, B. Kim, S. Hwang, C. P. Hong, Y. Yoon, G. Lee, V. H. Le, S. Bok, G. O. Ahn, J. Lee, Y. S. Gho, E. Chung, S. Kim, M. H. Jang, S. J. Myung, M. J. Kim, P. T. So, and K. H. Kim, "Moxifloxacin: Clinically compatible contrast agent for multiphoton imaging," Sci. Rep. **6**(1), 27142 (2016).
30. W. H. Jang, S. Shim, T. Wang, Y. Yoon, W. S. Jang, J. K. Myung, S. Park, and K. H. Kim, "In vivo characterization of early-stage radiation skin injury in a mouse model by two-photon microscopy," Sci. Rep. **6**(1), 19216 (2016).
31. V. Ross, G. Naseef, G. Lin, M. Kelly, N. Michaud, T. J. Flotte, J. Raythen, and R. R. Anderson, "Comparison of responses of tattoos to picosecond and nanosecond Q-switched neodymium: YAG lasers," Arch. Dermatol. **134**(2), 167–171 (1998).
32. S. Lee, J. H. Lee, J. H. Park, Y. Yoon, W. K. Chung, H. Tchah, M. J. Kim, and K. H. Kim, "In vivo 3D measurement of moxifloxacin and gatifloxacin distributions in the mouse cornea using multiphoton microscopy," Sci. Rep. **6**(1), 25339 (2016).
33. D. D. Ho, R. London, G. B. Zimmerman, and D. A. Young, "Laser-tattoo removal--a study of the mechanism and the optimal treatment strategy via computer simulations," Lasers Surg. Med. **30**(5), 389–397 (2002).
34. F.-J. Leu, C.-L. Huang, Y.-M. Sue, S.-C. Lee, and C.-C. Wang, "Effects of tattoo ink's absorption spectra and particle size on cosmetic tattoo treatment efficacy using Q-switched Nd:YAG laser," Lasers Med. Sci. **30**(1), 303–309 (2015).
35. C. R. Taylor, R. R. Anderson, R. W. Gange, N. A. Michaud, and T. J. Flotte, "Light and electron microscopic analysis of tattoos treated by Q-switched ruby laser," J. Invest. Dermatol. **97**(1), 131–136 (1991).
36. J. E. Ferguson, S. M. Andrew, C. J. Jones, and P. J. August, "The Q-switched neodymium:YAG laser and tattoos: a microscopic analysis of laser-tattoo interactions," Br. J. Dermatol. **137**(3), 405–410 (1997).

Biomedical Optics EXPRESS

37. L. G. Ng, J. S. Qin, B. Roediger, Y. Wang, R. Jain, L. L. Cavanagh, A. L. Smith, C. A. Jones, M. de Veer, M. A. Grimbaldeston, E. N. Meeusen, and W. Weninger, "Visualizing the neutrophil response to sterile tissue injury in mouse dermis reveals a three-phase cascade of events," J. Invest. Dermatol. **131**(10), 2058–2068 (2011).
38. I. Saytashev, R. Glenn, G. A. Murashova, S. Osseiran, D. Spence, C. L. Evans, and M. Dantus, "Multiphoton excited hemoglobin fluorescence and third harmonic generation for non-invasive microscopy of stored blood," Biomed. Opt. Express **7**(9), 3449–3460 (2016).

1. Introduction

A tattoo is a form of body art by inserting ink into the skin dermis. There are demands for removing undesired tattoos by cosmetic or medical needs. Currently, the removal of tattoo pigments is achieved by pulse laser treatment. The pulse lasers emit wavelengths optimal to target specific chromophores within a tattoo and generate selective photothermolysis while minimizing collateral damage. The commonly used pulse lasers for tattoo removal are Q-switched lasers producing nanosecond (ns) pulse durations of approximately 5 – 100 ns at various wavelengths such as ruby (694 nm), alexandrite (755 nm), and Nd:YAG (532 nm and 1064 nm) lasers. Picosecond (ps) pulse lasers, which have shorter pulse durations of 350 – 750 ps, have been developed recently [1–5]. The logic is that ns pulse duration might be too long for effective photothermolysis of small tattoo particles having thermal relaxation time (TRT) in ps ranges. These ps pulse lasers have shown better performance than ns lasers in either tattoo clearance per treatment session or the pain level in both preclinical studies [6] and clinical studies [7, 8]. Currently tattoo laser treatments are usually performed in multiple sessions with several weeks apart [9]. Influencing factors for determining the number of laser treatment include skin type, location, color, amount of ink, scarring or tissue change, and layering [10]. At each session, a portion of the tattoo pigment particles is fragmented, and the body removes the fragments over the course of several weeks. The amount of time required for the removal of a tattoo and the degree of removal varies depending on each individual.

Although laser tattoo removal treatment is regarded as safe, both temporary and permanent side effects do occur. Temporary side effects include pain, erythema, crusting, pinpoint bleeding, blistering, swelling, infection, and pigmentary disorders [11]. Permanent side effects include scarring, hypo- or hyper-pigmentation, and color change of tattoo pigment [9, 12]. A survey on the side effects of laser tattoo treatment reported a significant rate of slightly visible scars (24%) or even important scarring (8%) [13]. Studies on laser-, tattoo-, host-dependent factors in laser treatment could potentially minimize their occurrences in actual clinical practices. To study the side effects of laser tattoo removal, *in vivo* preclinical animal model studies are suitable, and non-invasive assessment methods are beneficial.

Optical imaging techniques, which provide high-resolution and non-invasive assessment of tattoo particles in the skin without skin biopsy, could be useful in both preclinical and clinical studies. Previously, various optical imaging techniques have been used for tattoo studies: optical coherence tomography (OCT), spatial frequency domain imaging (SFDI), reflectance confocal microscopy (RCM), and third-harmonic generation (THG). OCT is a 3D non-invasive optical imaging technique based on light reflection and depth resolved detection [14]. OCT visualized the 3D distribution of light absorbing pigments in human volunteers [15]. SFDI is a wide-field modulated imaging technique measuring optical properties such as scattering and absorption coefficients [16]. SFDI provided spatially resolved optical properties of multi-colored tattooed skin and non-tattooed skin of *in vivo* volunteers allowing quantitative assessment of the laser treatment [17]. RCM is a high-resolution 3D non-invasive microscopy based on the light reflection [18]. RCM has been used to image clustered or diffused pigment of various types of tattoo ink accumulated under the basement membrane of the skin [19]. Third-harmonic generation (THG) microscopy is another high-resolution 3D microscopy based on nonlinear THG interaction [20, 21]. THG showed potentials in tattoo particle detection in both cellular level and in mouse model *in vivo* [22].

Two-photon microscopy (TPM) is a high-resolution 3D fluorescence microscopy technique based on two-photon excitation of fluorophores [23, 24]. With advantages of

Biomedical Optics EXPRESS

minimal photo-damage and high imaging depths, TPM has been used in various *in vivo* studies including the skin [25, 26]. Since TPM contrast is based on fluorescence, TPM can visualize cells in the skin with better contrast compared to other imaging techniques, and has advantages in tracking the treatment effects in animal model studies. Additional fluorescence labelling techniques such as immunohistochemistry could be used to achieve molecular specificity or high contrast imaging [27, 28]. Moxifloxacin, an antibiotic to prevent or treat infection, could be used to label cells within tissues non-specifically *in vivo* [29]. Therefore, TPM may be useful for studying the effects of laser treatment in preclinical animal models *in vivo* by visualizing cells and tattoo particles longitudinally, and by analyzing more detailed molecular mechanisms.

In this study, TPM was used to visualize the laser treatment effects on tattoo particles in both phantom specimens and *in vivo* mouse models. Fluorescent tattoo particles were used for TPM visualization, and ns and ps lasers at 532 nm were used for laser treatment. In phantom specimens, TPM was used to assess the changes of individual tattoo particles by tracking them before and after the laser treatment, and the results were compared with those of field emission scanning electron microscopy (FE-SEM). TPM based method was used to measure the treatment efficiency of the ns and ps pulse lasers. In the mouse model, TPM was used to observe the effects of laser treatment on tattoo particles and dynamic cell behaviors in the skin.

2. Materials and methods

2.1 Characterization of fluorescent tattoo ink

A fluorescent tattoo ink (Purple, UV Blacklight tattoo, Eternal tattoo) was used for both tattoo phantom specimens and mouse models. The tattoo ink was analyzed in terms of size, shape, and optical properties, and the results are shown in Fig. 1. A FE-SEM (JSM-7401F, JEOL) image of the tattoo ink is shown in Fig. 1(a). The tattoo ink consisted of various sized particles, ranging approximately from 80 nm to 4 μm in diameter. Particles over several hundred nanometers in diameter had spherical shapes, while smaller ones had irregular shapes. Using energy dispersive spectroscopy (EDS), the composition of the tattoo ink was analyzed to be C(83.34%), N(8.15%), O(1.33%), Na(0.24%), S(0.38%), Fe(0.16%) and Co(0.16%). Fluorescence emission spectra of the tattoo ink at various two-photon excitation wavelengths are shown in Fig. 1(b). The fluorescence spectra were visible from approximately 550 nm to 700 nm with the peak at approximately 610 – 620 nm.

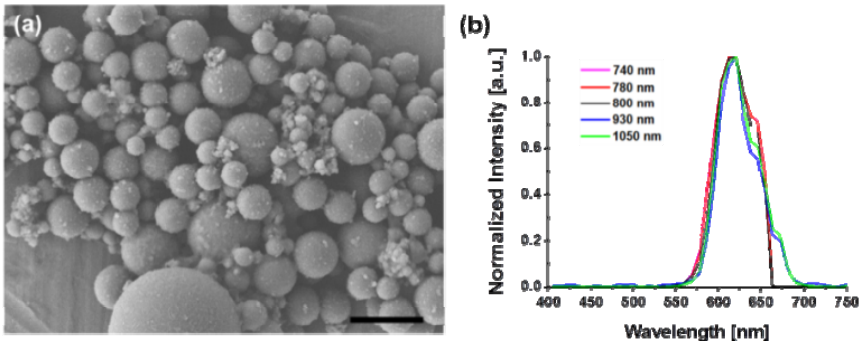

Fig. 1. Characterization of the fluorescent tattoo ink. (a) A FE-SEM image of the tattoo ink consisted of various sized particles. Scale bar indicates 2 μm. (b) Fluorescence emission spectra of the tattoo ink at various two-photon excitation wavelengths.

2.2 Sample preparations

In order to track the effects of laser treatment on individual tattoo particles, phantom specimens (n = 3) containing tattoo particles were prepared. The phantom specimens were

Biomedical Optics EXPRESS

prepared by the following procedure. (1) Tattoo ink was diluted in distilled (DI) water in 1:10 ratio and mixed with 10% agarose gel in 1:10 ratio using a magnetic stirrer. (2) Mixture of tattoo ink and agarose gel was placed on microscope well slides. (3) Two short pieces of hair were placed at the center of the mixture forming a cross as the reference for laser treatments and TPM imaging. (4) The mixture was covered with microscope cover glasses and was sealed with nail polisher. Pulse laser treatment was performed at the crossed region of the two short pieces of hair in order to reduce possible miss treatment.

All animal experimental procedures were conducted in accordance with institutional guidelines and regulations, and approved by the Institutional Animal Care & Use Committee at POSTECH (POSTECH-2015-0030-R1). Hairless mice (SKH1-HrHr, 6 weeks, female, OrientBio) were prepared for *in vivo* mouse experiments. Mice were kept under controlled conditions with access to food and water *ad libitum*. For the mouse model, tattoo ink was inserted in the skin dermis of the hindlimb using a 13RM tattoo needle. Mice were anesthetized using a face mask administering gas mixture of 1.5%/vol isoflurane (Terrel, Piramal) and medical grade oxygen during the tattooing procedure. During anesthesia, body temperature was maintained at 37 °C by using a temperature controlled heating plate (Chamlide TR, Live Cell Instrument). After tattooing, mice were allowed to rest and recover for at least 2 – 3 weeks before pulse laser treatment or TPM imaging. During *in vivo* TPM imaging, mice were anesthetized by using the same gas mixture and the hindlimbs were gently fixed by using a custom-made holder to minimize the breathing motion [30].

2.3 Pulse lasers

Two Q-Switched Nd:YAG lasers with ns (SPECTRA XT PLUS, Lutronic) and ps (PICO + 4, Lutronic) pulse durations were used for tattoo treatment. Laser specifications and experimental conditions of the ns and ps pulse lasers are described in Table 1. The phantom specimens were treated with laser fluences of 1 – 4 J/cm^2 and 0.5 – 2 J/cm^2, for the ns and ps lasers, respectively. Animal mouse models were treated with laser fluences of 1 J/cm^2 and 0.5 J/cm^2, for the ns and ps lasers, respectively. Number of laser treatments for the phantom specimens and *in vivo* animal mouse models were 5 shots and 1 shot, respectively. Fluences of the ps laser were selected to be smaller than those of the ns laser, based on clinical reports that ps lasers showed higher treatment efficiency compared to ns lasers [31]. A different ns pulse laser (RevLite, Cynosure) was used for the longitudinal TPM imaging of dynamic cell behaviors of the *in vivo* mouse model study. The laser treatment conditions were 532 nm wavelength, 5 – 20 ns pulse width, 2 mm spot size, 1 shot, and 3 J/cm2 fluence.

Table 1. Laser specifications and experimental conditions of ns and ps pulse lasers

	ns pulse laser	**ps pulse laser**
model	SPECTRA XT PLUS (Lutronic)	PICO + 4 (Lutronic)
pulse duration	5 – 10 ns	750 ps
spot size	3.3 mm	3.3 mm
wavelength	532 nm	532 nm
fluence	1, 2, 3, 4 J/cm^2	0.5, 1.0, 1.5, 2.0 J/cm^2

2.4 Two-photon microscopy (TPM)

A commercial TPM (TCS SP5 II MP, Leica) was used for this study. TPM was equipped with Ti-Sapphire laser (Chameleon Vision II, Coherent) with specifications of 140 fs pulse width and 80 MHz repetition rate. A 25 × objective lens (HCX IRAPO L25 × , NA 0.95 W, Leica) was used. For phantom specimen study, excitation wavelength of 780 nm was used, and the excitation power for TPM imaging was approximately 8 mw at the sample. Emission light was spectrally resolved by using 4 detection channels consisting of a set of dichroic mirrors of 495 nm, 560 nm, 620 nm and band-pass emission filters of 457/50, 525/50, 585/40, and

Biomedical Optics EXPRESS

650/50. TPM images consisting of 1024 pixels × 1024 pixels were acquired at approximately 0.2 frames/sec, and the imaging field of view (FOV) was 103 μm × 103 μm in the x-y plane. 3D images were acquired with a stepwise increment of 0.4 μm in the z direction. Image pixel sizes were set to be smaller than the resolution of TPM for the analysis of tattoo particle size. The acquired images were presented in black-white colormap. TPM 3D volumetric images were presented as the maximum intensity projection images of tattoo particles in the focal plane.

For the mouse model imaging, excitation wavelength of 780 nm was used for autofluorescence (AF) based TPM imaging and the emission signals were spectrally resolved with 4 channels by using a set of dichroic mirrors of 495 nm, 560 nm and 620 nm and band-pass emission filters sets of 457/50, 525/50, 585/40, and 650/50. The sensitivities of 4 NDD PMT channels were manually adjusted to compensate the difference in the intensities of AF and tattoo particle fluorescence. Detection sensitivities of long wavelength channels such as 585/40 and 650/50 were decreased. TPM images consisting of 1024 pixels × 1024 pixels were acquired, and the imaging speed was approximately 0.2 frames/sec. The FOV and axial increment size for 3D TPM imaging were 206 × 206 μm and 1.5 μm or 2 μm, respectively. The acquired images were displayed in pseudo-colors of blue (457/50), green (525/50), yellow (585/40), and red (650/50). For monitoring tattoo particle changes and cellular responses in the mouse model *in vivo*, cells in the skin were labeled by using a fluorescence contrast agent, moxifloxacin. Moxifloxacin is an FDA approved antibiotic to prevent and treat bacterial infection, and its usage as a cell labeling agent for TPM imaging was demonstrated with the benefits of clinical compatibility, strong fluorescence, and high accumulation inside cells [29, 32]. Moxifloxacin ophthalmic solution (Vigamox, Alcon Laboratories, Fort Worth, US) was topically administered on the gently tape-stripped mouse hindlimb skin for 20 min in 12.4 mM concentration before TPM imaging. For moxifloxacin based TPM imaging, excitation wavelength of 780 nm was used and the emission signals were spectrally resolved with 4 channels by using a set of dichroic mirrors of 455 nm, 505 nm and 560 nm and band-pass emission filters sets of 535/30, and 585/40. The acquired moxifloxacin and tattoo fluorescence were presented in pseudo-colors of blue (– 455 nm), green (455 – 505 nm and 520 – 550 nm), and red (565 – 605 nm). Fluorescence from moxifloxacin and tattoo particles were mostly detected from PMT channel 2, 3 and PMT channel 4, respectively. During autofluorescence TPM imaging, the excitation power ranged approximately between 25 mW to 56 mW depending on the depth. For moxifloxacin based time-lapse TPM imaging, excitation power was approximately 19 mW at the sample. Dynamic behavior of cells in the skin tissues was monitored by time-lapse TPM imaging with approximately 15 second interval in between.

3. Results

3.1 TPM analysis of tattoo particle fragmentation by laser treatment

Effects of laser treatment on tattoo particles were captured by TPM imaging of the same particles before and after the treatment, and the results are shown in Fig. 2. Phantom specimens containing tattoo particles were treated by the ns and ps lasers with high enough laser fluence levels of 4 J/cm^2 and 2 J/cm^2, respectively. TPM results of the ns laser before and after the treatment are shown in Figs. 2(a) and 2(b) and those of the ps laser are shown in Figs. 2(c) and 2(d), respectively. TPM images before the laser treatment show sparsely distributed tattoo particles. Before the laser treatment, tattoo particles were spherical in shape. TPM could resolve the various sized tattoo particles, ranging from 0.6 μm to 4 μm in diameter. Particles diameter smaller than 0.6 μm were neglected in the analysis, because TPM could not detect the shape changes after the laser treatment. TPM images after the laser treatments showed the shape changes. Zoomed images of representative individual tattoo particles showed the changes of tattoo particles clearly. Tattoo particles were expanded and

Biomedical Optics EXPRESS

fragmented with hollow centers. Fragmentation patterns of tattoo particles were similar in both the ns and ps laser treated phantom specimens.

Morphological changes of tattoo particles detected by TPM after the laser treatment were confirmed by FE-SEM imaging, and results are shown in Fig. 3. The aqueous solutions of tattoo particles diluted in DI water were treated by the ns and ps lasers with laser fluence of 4 J/cm^2 and 2 J/cm^2, and the results are shown in Figs. 3(a), 3(b) and Figs. 3(c), 3(d), respectively. Two representative enlarged images of fragmented tattoo particles, marked with black-dashed-box in Fig. 3(a) and 3(c), are shown in Fig. 3(b) and 3(d), respectively. After the laser treatment, tattoo particles appeared to be expanded, crushed, and torn as marked with yellow-arrows. The fragmentation patterns were similar in both the ns and ps pulse lasers. Shape changes in FE-SEM images were consistent with those in TPM images in Fig. 2(b) and 2(d). Some intact tattoo particles were visible in FE-SEM images after the laser treatment as marked with red-arrows. This might be because the laser treatment was performed on the aqueous solutions of tattoo particles diluted in DI water and only some portion of tattoo particles might have been affected by the laser.

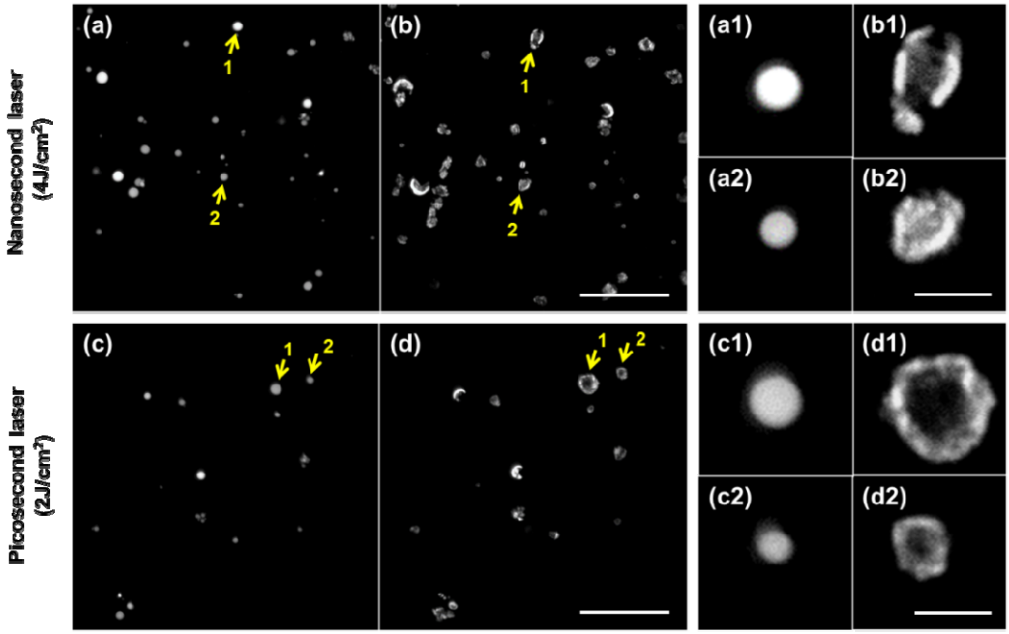

Fig. 2. Representative TPM images of tattoo particles before and after the laser treatment. (a, b) TPM images of tattoo particles before and after the ns laser (4 J/cm^2) treatment. (c, d) TPM images of tattoo particles before and after the ps laser (2 J/cm^2) treatment. Image sets on the right shows zoomed images of selected particles marked with yellow-arrows 1 and 2, respectively. Scale bars in (a – d) and in zoomed images indicate 30 μm and 5 μm, respectively.

Biomedical Optics EXPRESS

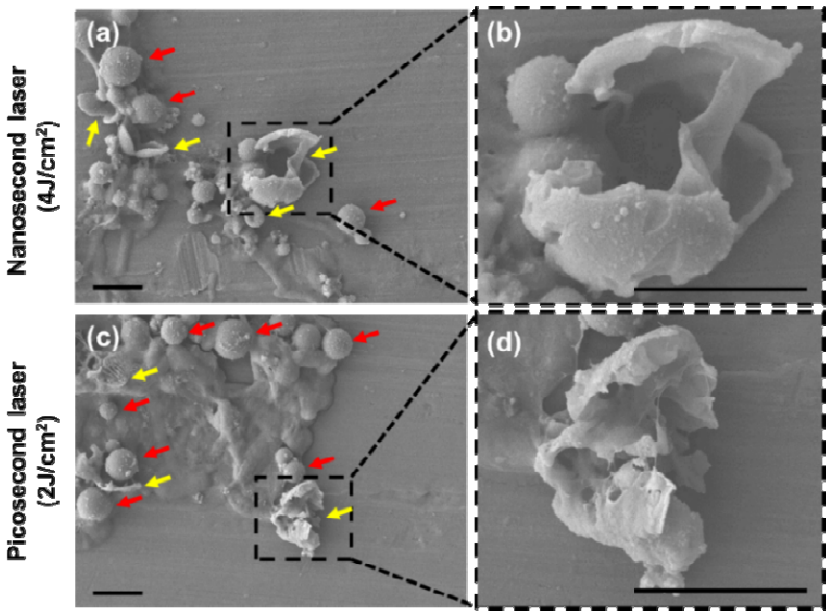

Fig. 3. FE-SEM images of tattoo particle after laser treatments. (a, b) FE-SEM images after ns laser (4 J/cm^2) treatment. (c, d) FE-SEM images after ps laser (2 J/cm^2) treatment. (b) and (d) are zoomed images of black-dashed-box regions in (a) and (c), respectively. Yellow- and red-arrows indicate fragmented and intact tattoo particles, respectively. Scale bars indicate 3 μm.

3.2 TPM assessment of laser treatment efficiency

Treatment efficiencies of the ns and ps pulse lasers were characterized by TPM imaging of phantom specimens after the treatment, and the results are shown in Fig. 4. The laser fluences used were 1, 2, 3, and 4 J/cm^2 for the ns laser and 0.5, 1.0, 1.5, and 2 J/cm^2 for the ps laser, respectively (Table 1). Dependence of laser treatment efficiency on tattoo particle sizes were roughly analyzed by dividing tattoo particles into two groups, smaller and larger than 2 μm in diameter. The criterion of 2 μm in diameter was chosen based on the convenience of TPM analysis. TPM results of the phantom specimen after ns and ps laser treatments of different laser fluences are shown in Figs. 4(a)–4(c) and Figs. 4(d)–4(f), respectively. For each pulse lasers, TPM images before and after the laser treatment are presented for comparison. At relatively high fluences of 3 and 4 J/cm^2 for the ns laser and 1.5 and 2 J/cm^2 for the ps laser, TPM images showed fragmentation of almost all the tattoo particles. However, at relatively low fluences of 1 and 2 J/cm^2 for the ns laser and 0.5 and 1 J/cm^2 for the ps laser, not all the particles were fragmented after the lasers treatment. The intact tattoo particles were mostly small ones, but some large ones were also intact. Intact tattoo particles after the treatment were marked with different colored arrowheads: yellow- and red-arrowheads for small and large particles, respectively.

Treatment efficiencies of the ns and ps lasers were quantitatively analyzed by tracking changes of individual tattoo particles, and results are shown in Figs. 4(c) and 4(f), respectively. The efficiency of laser treatment was measured by the ratio of the number of fragmented particles to the total number of particles. In case of the ns laser, the treatment efficiency of large particles was almost 100% at all the applied laser fluences, while the treatment efficiency of small particles was less than 100% and was proportional to the treated laser fluence. The treatment efficiency of small particles at relatively low fluences of 1 and 2 J/cm^2 was approximately 60% and 80%, respectively. In case of the ps laser, the treatment efficiency of large particles was approximately 100% at the fluences of 1.0 J/cm^2 or higher. However, the treatment efficiency of large particles dropped to approximately 50% at 0.5 J/cm^2. The treatment efficiency of small particles was less than 100% at all the applied laser

Biomedical Optics EXPRESS

fluences and was proportional with the treated laser fluence. At equal laser fluences of 1.0 J/cm^2, treatment efficiency of the ps laser (approximately 80%) was higher than the ns laser (approximately 60%). The ps laser (1.0 J/cm^2) showed similar treatment performance (approximately 80%) to the ns laser with approximately half the ns laser flucence (2.0 J/cm^2). Both the ns and ps lasers fragmented larger tattoo particles better than smaller ones.

3.3 TPM visualization of laser treatment effects in mouse skin in vivo

The effect of laser treatment on tattoo ink particles in the in-vivo mouse skin was visualized by TPM. TPM imaging was conducted before and 6 hours after the laser treatment and results are shown in Figs. 5(a), 5(c) and 5(b), 5(d), respectively. Results of the ns and ps laser treatments are shown in Figs. 5(b) and 5(d), respectively. TPM images showed tattoo ink particles in the skin dermis, at approximately 50-80 μm deep from the surface. Zoomed images of the yellow-dashed-box regions in Figs. 5(a)–5(d) are shown in Figs. 5(a1)–5(d1) in order to show tattoo particles more clearly. Laser fluences of 2 J/cm^2 and 1 J/cm^2 for the ns and ps lasers were used, respectively. *In vivo* mouse TPM images before the laser treatment showed densely distributed tattoo particles in the skin dermis. Most of tattoo particles were clustered while some were scattered. Tattoo particles were spherical in shape similar to those seen in the phantom specimens (Figs. 2(a), 2(c) and Figs. 4(a), 4(d)) and FE-SEM (Fig. 1(a)) results. Particles out-of-focus looked blurry due to optical aberration induced by irregularity of refractive index. TPM images 6 hours after laser treatment showed the expansion and fragmentation of tattoo particles, similar to those seen in the phantom specimens (Figs. 2(b), 2(d) and Figs. 4(c), 4(e)) and FE-SEM (Fig. 3) results. The fragmentation patterns were similar in both the ns and ps laser treatments. Additionally, TPM images showed some blue colored structures whose fluorescence was captured in 457/50 nm detection channel. These blue structures could be either rare tattoo particles expressing blue fluorescence or cells expressing AF in the skin dermis. Detailed explanation was included in discussion section.

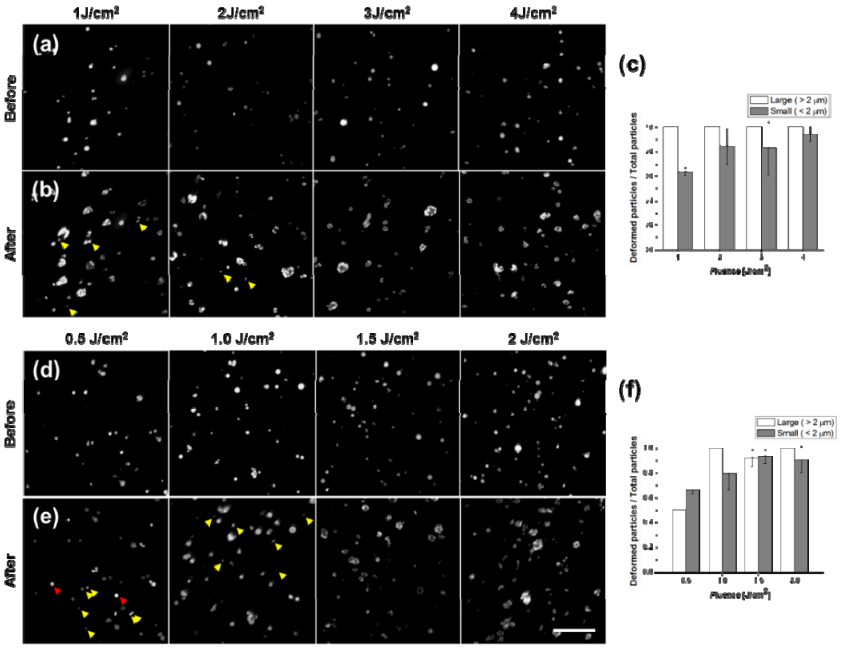

Fig. 4. TPM images of tattoo particles before and after the laser treatment at various laser fluences and the efficiency analysis of the ns and ps lasers in tattoo particle fragmentation. (a – c) ns laser treatment at 1, 2, 3, and 4 J/cm^2 fluences. (d – f) ps laser at 0.5, 1, 1.5, and 2 J/cm^2 fluences. Yellow- and red-arrowheads indicate intact small and large tattoo particles, respectively. (c, f) Quantitative treatment efficiency of the ns and ps lasers, respectively.

Biomedical Optics EXPRESS

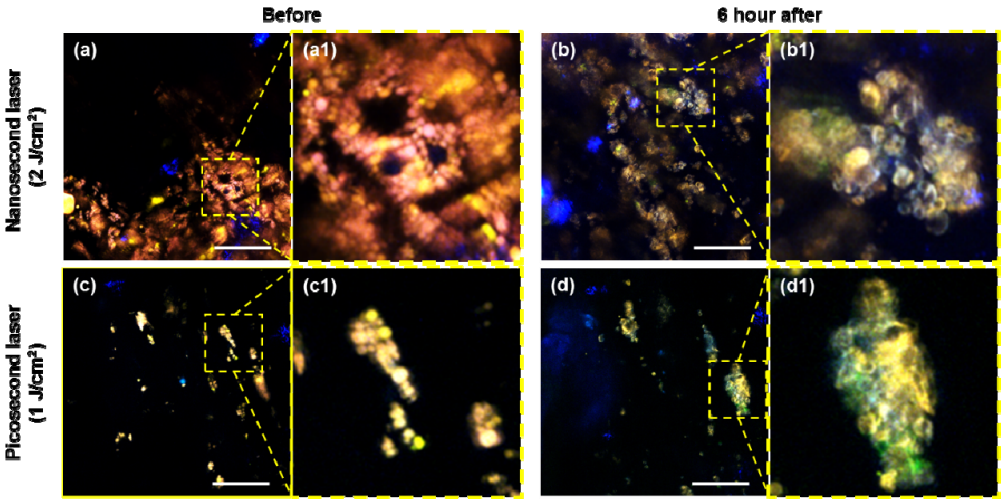

Fig. 5. TPM images of tattoo particles in the mouse skin before and 6 hours after the treatment *in vivo*. (a, b) TPM images before and after the ns laser (2 J/cm^2) treatment. (c, d) TPM images before and after the ps laser (1 J/cm^2) treatment. Scale bars indicate 50 μm.

TPM was used to capture the dynamic changes of microenvironment in the skin after the laser treatment. A different ns pulse laser (RevLite, Cynosure) was used in this experiment, due to unavailability of the other laser. Longitudinal time-lapse TPM imaging was conducted before and 6 hours after the ns laser treatment with 3 J/cm^2 fluence and the results are shown in Figs. 6(a)–6(c) and Figs. 6(d)–6(h), respectively. These time-lapse TPM images show the skin dermis at approximately 50 – 80 μm deep from the surface. Since moxifloxacin and tattoo particles had different fluorescence emission spectra, their fluorescence signals were collected at different spectral channels and were color coded in different colors: red and green colors for tattoo particle and moxifloxacin fluorescence, respectively. With moxifloxacin labelling, TPM showed cellular structures in the skin in high contrast. A representative *in vivo* TPM image before the laser treatment is shown in Fig. 6(a). TPM images captured the migration of some cells in Fig. 6(a), and the migration tracks of these cells were depicted in different colored solid-lines. Enlarged time-lapse images of two white-box regions in Fig. 6(a) are shown in Figs. 6(b1)–6(b3) and Figs. 6(c1)–6(c3), respectively. The time stamps in the enlarged images are relative time points with respect to the starting time of the time-lapse imaging. Locations of migratory cells at different time points are depicted with different colored arrowheads in the enlarged time-lapse images. Vasculatures were visible by surrounding moxifloxacin labeled endothelial cells and some cells inside the vasculatures. Vasculatures were marked with white-dashed-lines for visibility. Before the laser treatment, tattoo particles were stationary during the longitudinal TPM imaging. Some tattoo particles appeared to be inside some moxifloxacin labeled cells, but these cells did not show much movement. Although there were some migratory cells in the skin, these cells did not contain tattoo particles inside.

Biomedical Optics EXPRESS

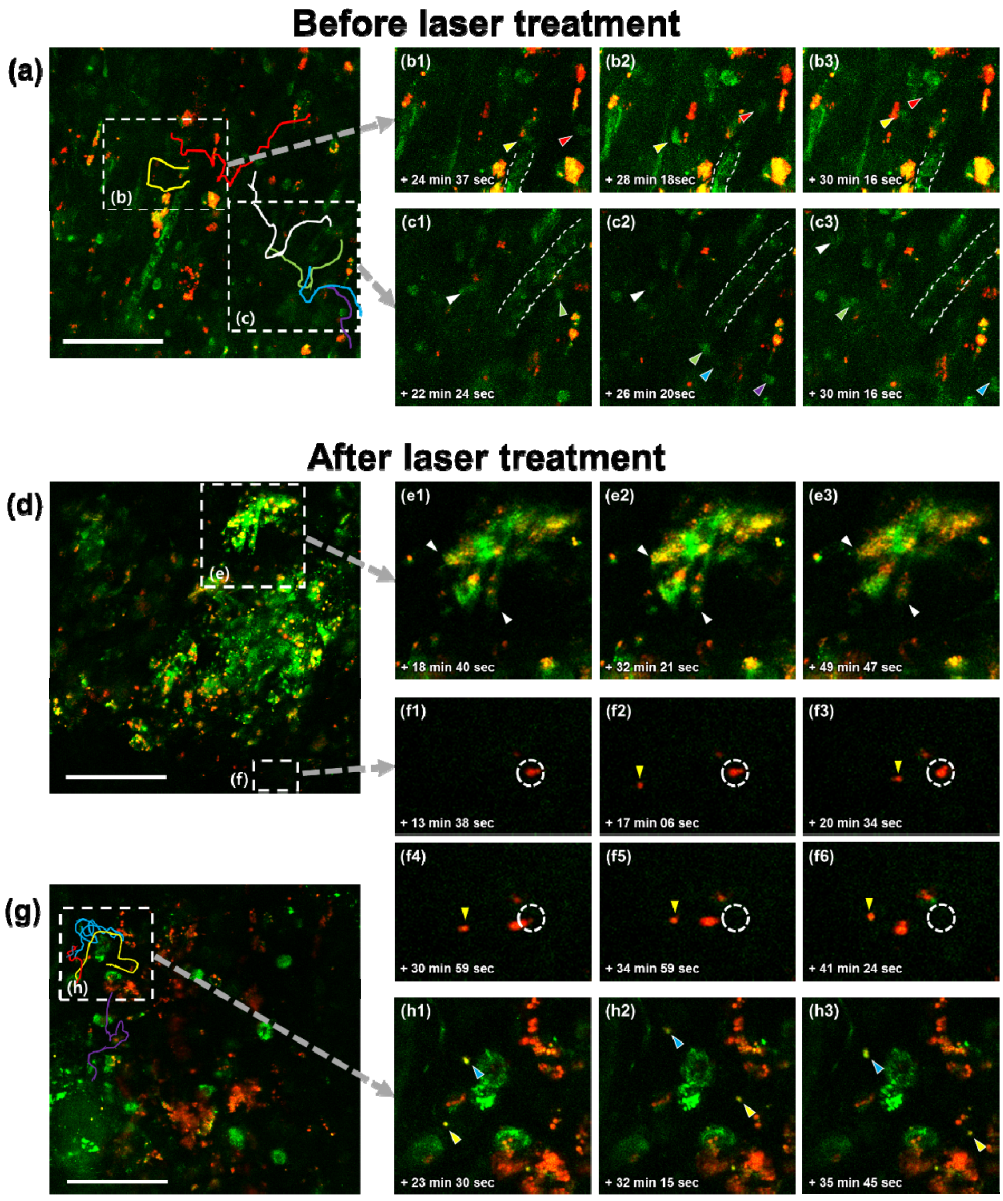

Fig. 6. Time-lapse TPM images of the mouse skin dermis before and after the ns laser treatment. (a – c) TPM images before the laser treatment (Visualization 1). (d – h) TPM images 6 hours after the laser treatment (3 J/cm^2) (Visualization 2, Visualization 3). Red and green colors in TPM images indicate tattoo and moxifloxacin fluorescence, respectively. Zoomed time-lapse TPM images show both tattoo particles and cells at different time points. Time stamps in the zoomed images depict relative time points with respect to the starting time of the time-lapse imaging. Scale bars indicate 100 μm.

TPM images in 6 hours after the laser treatment showed dynamic changes inside the skin. Tattoo particles were found inside either slowly migrating large cells or relatively fast migrating small cells in Figs. 6(d) and 6(g). Enlarged time-lapse images of two white-dashed-box regions in Fig. 6(d) at different time points are shown in Figs. 6(e1)–6(e3) and Figs. 6(f1)–6(f6), respectively. The time stamps in the enlarged images are relative time points with respect to the starting time of the time-lapse imaging. White-arrowheads in Figs. 6(e1)–6(e3)

Biomedical Optics EXPRESS

marked an edge of slowly migrating tattoo particle containing large cells at different time points. Yellow-arrowheads in Figs. 6(f1)–6(f6) marked relatively fast migrating tattoo particles, which happened by movement of the tattoo containing cells. In the same time-lapse images, a white-dashed-circles depicted the initial position of another tattoo particle cluster at the first imaging time point in Fig. 6(f1). This tattoo cluster was visible within the white-dashed-circle at the next two imaging time points as can be seen in Figs. 6(f2) and 6(f3). At the later time points the tattoo cluster migrated out of the initial area as depicted in Figs. 6(f4)–6(f6). Migration of small cells and tattoo particles at a different neighboring location is shown in Fig. 6(g). Migration tracks of these cells are depicted with different colored solid-lines in Fig. 6(g). Enlarged time-lapse images of a white-dashed-box region in Fig. 6(g) at different time points are shown in Figs. 6(h1)–6(h3), and the locations of small migratory cells are depicted with different colored arrowheads in the enlarged time-lapse images. TPM images also showed intact tattoo particles, after the laser treatment. It could be because a different ns pulse laser was used in this experiment and the actual output of the laser might be different from the laser setting. However, TPM visualized the increased activity of immune cells and tattoo particles after the laser treatment.

4. Discussion

In this study, TPM was used to visualize laser treatment effects on tattoo particles in both tissue phantom specimens and *in vivo* mouse models. TPM visualized the shape changes of tattoo particles after the treatment: tattoo particles were expanded and fragmented with hollow centers after the laser treatment. TPM could resolve various sized tattoo particles, ranging from 0.6 μm to 4 μm in diameter. Fragmentation efficiencies of the ns and ps pulse lasers were qualitatively and quantitatively analyzed by tracking the changes of individual tattoo particles in phantom specimens. In the mouse model, TPM visualized tattoo particle clusters in the skin and captured dynamic cell behaviors as the effect of laser treatment. After the laser treatment, tattoo particles were detected inside either slowly migrating large cells or relatively fast migrating small cells.

Previously, the effects for laser tattoo treatment have been analyzed by either computer simulations, tissue histology, or electron microscopy. Computer simulation analyzed the minimum laser fluence required for fragmentation of tattoo particles, and the optimal laser pulse width for efficient treatment and the dependency of particle sizes [33]. Electron microscopy showed the effects of laser treatment on tattoo particles in tissues with high resolution [34]. In this study, TPM was used to analyze various factors in laser tattoo removal such as laser fluence, laser pulse duration, and particle size experimentally. TPM based experiments showed dependency of laser treatment efficiency on those factors, and the TPM results were consistent with previous reports.

Usage of TPM for the characterization of tattoo laser treatment has several advantages over conventional analysis methods such as tissue histology or electron microscopy. First, with optical sectioning capability of TPM, 3D volumetric imaging is possible. This allows the observation of changes in tattoo particles and tissue microenvironment without information loss encountered in conventional tissue histology. Second, TPM is non-invasive technology allowing longitudinal *in vivo* study. Unlike conventional electron microscopy or tissue histology, where tissue is excised, long term monitoring of identical samples is possible. Third, time-lapse imaging is possible allowing the detection of dynamic changes in real time. Migration of cells or tattoo particles in the skin dermis could provide detailed information about tattoo phagocytosis or immune response after laser treatment. Forth, since TPM is based on fluorescence contrast, additional fluorescence labelling technique could also be used. Cells imaged in the skin dermis could be identified with the use of immunohistochemistry. In doing so, more in-depth study of the clearance mechanism of tattoo particle in *in vivo* preclinical model might be possible. Fifth, TPM can visualize cells and some components of extracellular matrix based on AF and second harmonic generation

Biomedical Optics EXPRESS

(SHG). SHG is a nonlinear optical phenomenon where excitation photons are combined to generate new photons twice the energy via interaction with a nonlinear material. SHG contrast in TPM can visualize collagen distribution in the skin dermis and it should be useful to study collagen damage during the laser procedure [34].

With the advantages of TPM, dynamic cell behaviors were observed in the time-lapse imaging. Before the laser treatment, migration of some cells was observed in the skin. However, these migrating small cells did not have tattoo particles inside them. Tattoo particles in the skin were mostly stationary during the longitudinal TPM imaging (Figs. 6(a)–6(c)). After the laser treatment, tattoo particles were detected inside the migrating immune cells. The relatively slowly migrating tattoo particle containing large cells (Fig. 6(e)) might be either macrophages, fibroblasts, or mast cells, which has been reported to contribute to the clearance of tattoo particles after laser treatment [35, 36]. The relatively fast migrating cells (Fig. 6(h)) might be neutrophils which is other immune cells contributing to the clearance of tattoo particles after laser treatment [37]. Although the migration of cell containing tattoo particles alone might not directly confirm the *in vivo* clearance of tattoo particles, it could confirm the active phagocytosis of tattoo particles by immune cells.

Autofluorescence based TPM images of tattoo particles in the mouse skin dermis in Fig. 5 showed some blue colored structures whose fluorescence was captured in 457/50 nm detection channel. These blue structures could be either rare tattoo particles expressing blue fluorescence or cells expressing AF in the skin dermis. The majority of the tattoo particles had fluorescence at approximately 610 – 620 nm, but a small portion of the particles expressed blue fluorescence. Round structures with strong blue fluorescence might be blue fluorescent tattoo particles. Structures expressing relatively weak blue fluorescence in the left side of Fig. 5(d) were cell clusters in the sebaceous glands based on the analysis of 3D TPM images and their morphologies. AF of cells appeared relatively equivalent to fluorescence of tattoo particles in these TPM images, because sensitivities of the 4 NDD PMT channels were adjusted to be compensate for the difference in fluorescence efficiency of AF and tattoo particles. Finally, the blue ones near tattoo particle clusters might be either blue tattoo particles or inflammatory cells recruited as the results of inflammation response.

Although TPM based assessment method of tattoo laser removal provided new information, this method had some limitations. First, the studies of tattoo treatment using TPM has limitation in applicable tattoo ink. Due to the basic contrast source of TPM, only fluorescent tattoo ink needs to be used. However, with a multimodal TPM and third harmonic generation (THG) microscopy system [38], simultaneous imaging of non-fluorescent tattoo particle and cellular structures may be possible. Non-fluorescent tattoo particles could be imaged with THG, while the dynamic cell behaviors could be imaged with TPM. Second, the fluorescent tattoo ink used in this study showed response to 532 nm but not to1064 nm pulse laser, hence the 532 pulse laser was used in the study. However, 532 nm is known to show significant laser-tissue interaction based on light absorption especially in either skin pigments or blood, which could cause unwanted tissue damage. Therefore, the treatment of pulse laser was performed in laser fluences level that did not show unwanted visible tissue damage. Such factors can be reduced with the use of tattoo particles that respond to 1064 nm laser. At 1064 nm, optical absorption of the skin pigments or blood is relatively low which may allow laser treatment with relatively higher fluence which may lead to higher treatment efficiency. Also at 1064 nm the optical attenuation is relatively lower, compared to 532 nm, allowing light penetration to deeper tissue, allowing laser treatments of deeply embedded tattoos.

5. Conclusion

In this study, two-photon microscopy (TPM) was used to assess the fragmentation of tattoo particles and dynamic changes in the skin after the tattoo laser treatment. TPM captured the fragmentation of individual tattoo particles by the laser treatment in phantom specimens and TPM results were confirmed by FE-SEM. In the mouse model, TPM visualized the effects of

Biomedical Optics EXPRESS

laser treatment such as the fragmentation of tattoo particles and dynamic cell behaviors in the skin. TPM based method would be useful for studying the detail process of laser tattoo removal treatment in the preclinical model.

Funding

This research was supported in part by Lutronic Corporation, and Korea Institute of Radiological and Medical Sciences (KIRAMS) funded by Ministry of Science, ICT and Future Planning, Republic of Korea (1711045573/50535-2017), and Engineering Research Center grant (No. 2011-0030075), Korea-Sweden Research Cooperation Programme (No. NRF-2014R1A2A1A12067510) of the National Research Foundation (NRF) funded by the Korean government (MEST), and grant(No. 2015-653) from Asan Institute for Life Sciences, Asan Medical Center, Seoul, Korea..